

# Computer Modeling and Simulation of Ground Penetrating Radar using Finite Difference Time Domain Code

J. Hebert<sup>1,2</sup>, T. Holzer D.Sc.<sup>1</sup>, T. Eveleigh PhD<sup>1</sup>, Dr. Shahryar Sarkani, PhD<sup>1</sup>, and J. Ball PhD<sup>2</sup>

<sup>1</sup> George Washington University Washington, D. C.

<sup>2</sup> Naval Surface Warfare Center Dahlgren Division, Dahlgren, VA

## Abstract

*Modeling and simulation results of a system analysis of Ground Penetrating Radars (GPR) using Finite Difference Time Domain (FDTD) techniques are presented. Performance issues with GPRs need to be isolated in order to optimize of the radar's ability to detect and identify buried objects. Using a system engineering approach, FDTD models were used to characterize the variables associated with the GPR to improve GPR detection process minimally affected by external sources of variability. These experiments make changes to the GPR's inputs while measuring the output response to identify issues and optimize performance. FDTD computer simulations produce idealistic environments that allow examination of the individual effects on the response. This paper provides a system engineering overview of the operations and processes of GPR systems and how MATLAB based FDTD computer simulations can be used to model and improve them. A plan for future work is presented.*

**Key Words:** System, Modeling, Simulation, GPR, System Engineering, FDTD

## 1 Introduction

A system analysis is performed to isolate and understand the factors that affect a GPR's ability to detect and identify buried objects. The use of FDTD computer models and simulations in the systems analysis enable GPRs to be designed to do what they should do. Many factors affect a GPR's ability to detect and identify subsurface objects. A major factor is the electrical characteristics of the object and of the material in which the object is buried. Although several attempts to use carefully prepared test sites to make measurements to understand the magnitude of these performance limiting effects have been made, a comprehensive system engineering based investigation has not been reported to date. This is due to the time and expense of preparation of configurations for measurement based investigations, and the lack of any reported system engineering efforts applied to GPR.

The effects of changing simple variables such as surface and soil constituent properties on the GPR radar's output are not separable. Often the effects are unidentifiable in measurements made under field conditions. A synthetic data set produced by FDTD computer simulations allows the separation of input variables to better understand their effects on the output response of the radar. These simulations produce idealistic environments and test configurations to allow close examination of the individual effects of these variables on the response. This paper presents a version of FDTD code that has been implemented in MATLAB to model and simulate a GPR's performance. This version of the code is intended for use by researchers to observe, analyze, and understand how different system input variables affect the GPR and its performance.

Modeling the GPR as a system using FDTD techniques allows a set of specially designed experiments where deliberate changes are made to the input variables so that changes in the output response can be observed and performance limiting issues can be easily identified. Three MATLAB models and simulations are presented in this paper: (1) a model for calculating the Fresnel reflection and transmission coefficients for perpendicular and parallel polarity incident waves as a function of grazing angle, (2) a one dimensional (1D) FDTD model for comparison with the Fresnel model, and (3) a three dimensional (3D) FDTD model to allow simulation of the response to the GPR of changing various inputs. The amount of energy that is reflected at the boundary of two media (e.g., soil and buried target) with different permittivity is given by the Fresnel coefficient. The changes in output response were observed while controlling various input variables. The initial results of controlling the conductivity and permittivity of the soil and targets are presented. Conductivity is a measure of a material's ability to conduct an electric current. Permittivity relates to a material's ability to transmit (or "permit") an electric field.

David Montgomery states that one of the applications of experiment design is the identification of design parameters that work well over a wide range of conditions in order to determine the design parameters that most impact product performance [1]. Variables to be

considered in simulation of the GPR as a system are: (1) radiated waveform, (2) depth of penetration versus frequency, (3) transmitter antenna type, (4) height and grazing angle, (5) surface, soil, and target properties, (6) target characteristics, (7) clutter (8) moisture content, (9) interference (10) receiver antenna type, (11) signal collection resolution and rate, (12) signal processing techniques, and (13) optimizing response of all input variables to maximize detection and reduce false alarm rate. Our initial research focused on two input variables that were found to greatly affect the GPR's output response: conductivity and permittivity. A detailed examination of the response of the system to changing these two input variables allowed for optimization to obtain the most accurate possible output response. The system engineering goal of this modeling and simulation effort is to define what a GPR system should be rather than applying a classical approach of determining of what a GPR can be.

## 2 GPR System Analysis

This section discusses the motivation for using the SE tools of modeling and simulation in the development of the System Engineering GPR computer model and the selection of FDTD techniques to perform the system simulations and analyses. Surface penetrating active sensors (SPAS), such as GPR, and ultrasound have hundreds of real world applications for their ability to "see into" and characterize solid and semi-solid substrates. As such, they are highly desirable functional components for a growing number of advanced systems. The computer models and mathematics for surface penetrating active sensors can be quite involved with only a few sensor models developed for specific instruments, for specific applications, and/or for specific environments of use. To date, no general sensor system characterization models exist that can deterministically characterize sensor technology or examine the parametrics, and tune in a response to an intended environment of use and a desired target resolving capability. The ability to deterministically match system sensing needs to SPAS capabilities would be of great interest to the systems engineer. At present, it is very difficult for all but the most highly trained experts to know what SPAS capabilities might work under what given set of conditions. This paper presents an extensible approach towards the allocation of sensing performance requirements to determined SPAS solution technologies.

The goal of this system engineering analysis is to identify GPR system deficiencies and what can be done to improve the system's performance. Five important steps in the system engineering process include: (1) critical needs are identified, (2) current capabilities are assessed, (3) new or existing capabilities are explored, (4) prototyping or modeling and simulation are implemented and (5) final system deployed. The FDTD model for this research facilitates the system analysis required by steps 2, 3, and 4.

This approach could provide the systems engineer with a requirements-driven solution synthesis by better characterizing and populating the architectural trade space

with valid SPAS alternatives that represent a range of possible SPAS solutions.

## 3 Radar Ground Penetrating

To analyze the GPR as a system we must first understand the components and functions of the GPR. This radar is used for the detection of objects buried below the surface. A GPR consists of a transmitting and receiving antenna, a source connected to the transmitting antenna, and signal processing equipment connected to the receiving antenna. The type of antennas, choice of the transmitted signal, and method of signal processing are all system variables that affect the output response and performance of the GPR. As such each is a candidate for optimization as part of the GPR's system architecture and design.

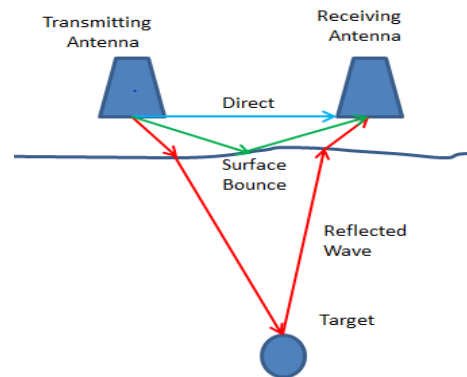


Figure 1. Schematic drawing of typical GPR.

Figure 1 shows a GPR system and operating environment with the signals that are generated by the system. Filtering out the interference caused by the direct and the ground bounce signals in order to see the reflection of the return from the target may be necessary. The operating environmental variables that must be modeled in a GPR simulation include the two antennas, the electrical characteristics: permittivity,  $\epsilon$ , conductivity,  $\sigma$ , and permeability,  $\mu$ , of the air above the surface, the subsurface, and the target. Other variables include the height above the surface of the antenna, the separation distance between the antenna, and the depth of the target. Most of these variables are related or dependent on the other variables such that modeling them one at a time would cause unaccounted for errors in the output response. The best that can be done is to control the variables one at a time, while including all the variables in the GPR model and simulation. The research presented here includes a three-dimensional, finite-difference time-domain (3D-FDTD) system analysis of the GPR that accounts for many of these variables simultaneously within the problem space.

Table 1. Relative permittivity,  $\epsilon_r$ , and EM velocity for selected geological materials

Material	$\epsilon_r$ : Davis and Annan (1969)	$\epsilon_r$ : Daniels et al (1995)	Velocity (m/ns)	Velocity (ft/ns)
Air	1	1	0.3	0.96
Distilled water	80		0.03	0.11
Fresh water	80	81	0.03	0.11
Sea water	80		0.03	0.49-0.57
Fresh water ice	3-4	4	0.15-0.17	0.35-0.49
Sea water ice		4-8	0.11-0.15	0.28-0.35
Snow		8-12	0.09-0.11	0.35-0.50
Permafrost		4-8	0.11-0.16	0.40-0.57
Sand, dry	3-5	4-6	0.12-0.17	0.18-0.31
Sand, wet	20-30	10-30	0.05-0.09	0.57-0.70
Sandstone, dry		2-3	0.17-0.21	0.31-0.44
Sandstone, wet		5-10	0.09-0.13	0.35-0.49
Limestones	4-8		0.11-0.15	0.37
Limestone, dry		7	0.11	0.35
Limestone, wet		8	0.11	0.25-0.44
Shales	5-15		0.08-0.13	0.33-0.40
Shale, wet		6-9	0.10-0.12	0.18-0.44
Silts	3-30		0.05-0.13	0.18-0.44
Clays	5-40		0.05-0.13	0.16-0.44
Clay, dry		2-6	0.12-0.21	0.40-0.70
Clay, wet		15-40	0.05-0.08	0.16-0.25
Soil, sandy dry		4-6	0.12-0.15	0.40-0.49
Soil, sandy wet		15-30	0.05-0.08	0.16-0.25
Soil, loamy dry		4-6	0.05-0.08	0.40-0.49
Soil, loamy wet		15-30	0.07-0.09	0.22-0.31
Soil, clayey dry		4-6	0.12-0.15	0.40-0.49
Soil, clayey wet		10-15	0.08-0.09	0.25-0.31
Coal, dry		3.5	0.16	0.53
Coal, wet		8	0.11	0.35
Granites	4-6		0.12-0.15	0.40-0.49
Granites, dry		5	0.13	0.44
Granites, wet		7	0.11	0.37
Salt, dry	5-6	4-7	0.11-0.15	0.37-0.49

One variable that has a large impact on a GPR's performance is the permittivity. Table 1 [2] shows the relative permittivity and electromagnetic wave velocity for common subsurface materials. The amount of energy that is reflected at the boundary of two media with different permittivity is given by the Fresnel coefficient. For air to soil with permittivity,  $\epsilon_r$ , and permeability,  $\mu_r$ , the index of refraction (Fresnel reflection coefficient) is described by:

$$n = \sqrt{\frac{\epsilon\mu}{\epsilon_0\mu_0}} = \sqrt{\epsilon_r \mu_r} \quad (1)$$

This relationship is used to illustrate the changes in the electromagnetic waves at the interface of two materials with different permittivity and permeability in the results section below. One observes that electromagnetic waves pass through the earth and the receiving antenna records the timing and magnitude of the arriving energy. A GPR image is actually an image directly related to the dielectric properties of the subsurface. The dielectric constant controls the velocity and the path of electromagnetic waves, including those reflected off objects below the surface.

### 3 FDTD Technique

FDTD techniques relate the surface currents and charges in a problem space that are modeled by Maxwell's curl equations which are:

$$\nabla \times \mathbf{E} = -\frac{\partial \mathbf{B}}{\partial t} \quad (2)$$

$$\nabla \times \mathbf{H} = \mathbf{J} + \frac{\partial \mathbf{D}}{\partial t} \quad (3)$$

These equations are used to develop a solution approach known as the finite difference formulation. A detailed development of the equations for the three dimensional version of the FDTD code is presented in a thesis by Williford [6]. Although the FDTD approach can be carried out both in the time and frequency domain, the model used for this research implements the time domain formulation. FDTD models the propagation and interaction of an electromagnetic wave in a region of space that may contain any object. This method is different from the integral equation method in that it analyzes the interaction of the incident wave with a portion of the structure at a given instant in time rather than solving the entire problem at once. Yee [6] first suggested the FDTD formulation for solving Maxwell's two curl equations (1) and (2), stating that the derivatives in these equations could be expressed as differences of the field values between neighboring positions, both temporally and spatially. These difference equations yield the values of the field at a given location in time and space if the values at all positions in the problem space are known at an earlier time.

The solution of an electromagnetic interaction problem by the FDTD technique is straight forward. For our system model, the problem space is divided into a lattice of uniform sized cells. As shown in Figure 3, the gridding procedure involves placing the components of the electric (E) and magnetic (H) fields around a unit cell and evaluating the field components at alternate half-time steps.

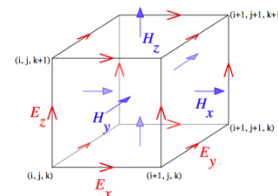


Figure 3. 3D Yee cell [13]

By alternating between the E and H fields, a central difference expression can be developed for both the space and time derivatives that maintains a higher degree of accuracy than either a forward or backward difference formulation. The problem solution proceeds by time-stepping throughout the problem space, repeatedly solving the finite difference form of Maxwell's two curl equations. In this fashion, the incident wave is tracked through the problem

space as it intercepts and interacts with the targets, at layer interfaces, and with other objects in the problem space.

Yee [6] developed the FDTD algorithm in 1966 as a method to compute the waveforms of pulses scattered from infinitely long, rectangular cross section, conducting cylinders Rymes [7] used FDTD to analyze data from direct lightning strikes to a NOAA C-130 aircraft. This code was later modified and used by Hebert and Sanchez-Castro [8] to analyze the data from inflight lightning strike measurements by a CV-580 aircraft and by Williford [5] to explore the validity of different boundary conditions using FDTD to model an F-16 aircraft. Williford, Jost, and Hebert [8] found using FDTD absorbing boundary conditions with FDTD produced better results than the perfectly electrically conducting (PEC) reflective boundary conditions originally used by Yee [6] but at the cost of longer run times.

Based upon these efforts, FDTD has been shown to be useful for the modeling and analysis of electromagnetic interaction with systems. These codes are easily adapted to a variety of materials in the problem space leading directly to their choice to analyze GPR data. In addition, nonlinearities and time-varying quantities can be represented in the problem space grid, if the needed equations can be written at the appropriate location. In addition, FDTD codes written in MATLAB are easily adapted to parallel processing and multi-processor systems.

## 4 3D-FDTD Models and Simulation

The FDTD code calculates the solutions to Maxwell's Equation in their differential form. FDTD solutions are simple and depending on the choice of time steps and grid lengths provide extremely accurate representations of the interaction of electromagnetic waves and materials with different constituent properties. Modeling using FDTD techniques allows the observation of changes in response due to changing input variables without the expensive cost of physical experiments.

There are many versions of the 3D-FDTD code. Some are readily available for download on the internet. Commercial versions of the code and versions that are reported in scholarly journals come in packages are not open source and are not available for researchers. For this reason, a GPR model and simulation program implementing FDTD techniques was developed in MATLAB.

Many different algorithms exist for target detection and identification, noise and interference suppression, removal of direct and air wave effects, and correction of attenuation losses. The input data for the research and comparison of these algorithms is provided by the FDTD techniques implemented in the MATLAB code.

Previous researchers have successfully used 3D-FDTD techniques to investigate some aspects of a GPR's performance [5, 11]. While helpful, these studies produced

only limited results. Under some physical soil conditions, the recognized landmine signature possesses high quality contrast while under other conditions no signature is detected. Fritzsche [3] demonstrated via modeling that GPR signals at 900 MHz would be strongly attenuated in moist soil. Trang [4] found through simulations and experiments with a GPR signals operating at 600-800 MHz that nonmetallic mines were easier to detect in moist soil.

The FDTD computer model implemented as part of this research facilitates the analysis of complex dielectric constant of soil and attenuation of GPR signals. In addition, the system model is capable of plotting the complex dielectric constant of soil coupled with the attenuation of GPR signals versus soil physical properties.

To predict the performance of electromagnetic sensors sub-systems, it is common practice to use models that estimate the soil's characteristics including dielectric properties. Trang found that no current model exists to completely describe all the electrical properties of a soil type [4]. Measurements to baseline GPR operational performance made at many sites worldwide are helpful but still leave a great deal unknown due to uncertainties caused by factors such as soil composition, layering, clutter, rock and other undesired artifacts recorded in the measurement. Alternatively, the FDTD computer models and simulations allow the variables associated with GPR system to be researched and characterized.

FDTD techniques model many variables that are controllable while some variables are not. Using FDTD synthetic data allows one to control what might otherwise be undefined or uncontrollable variables. The system engineering goal for the simulations is to find bounds for the input values of the uncontrollable variables which make the systems performance predictable and manageable. Thus a GPR system design can be optimized to effectively handle a wider variety of operational conditions

Figure 2 shows a B-mode image of buried pipes. A B-mode image is produced by sweeping a narrow beam while transmitting pulses and detecting echoes along a series of closely spaced scan lines. The algorithm for B-mode image simulation and processing includes calculation of the amplitude and two-way time delay of a signal reflected from each layer of a multi-layered media; simulation of echo signals, clutters, speckle and impulse noise; construction of synthetic range profile; and image formation.

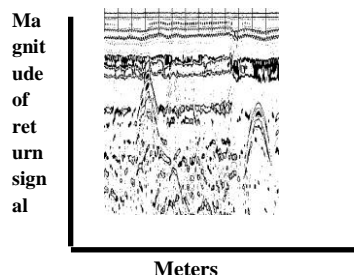


Figure 2. Example of a B mode plot  
 Belli, Rappaport, Udall, Hines and Wadia-Fracetti [10] provided an excellent example of a subsurface tunnel modeled in FDTD, as illustrated in Figures 4 and 5.

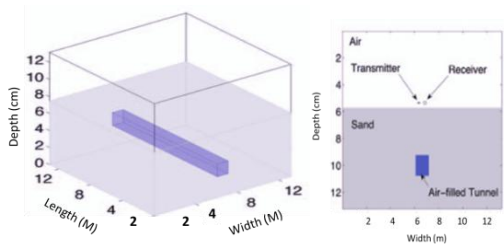


Figure 4. (a) 3D tunnel geometry, and (b) Detail of  $y - z$  plane indicating sensor location when  $\theta = 0^\circ$  [11]

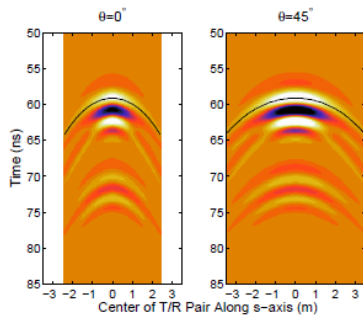


Figure 5. 3D-FDTD simulated B-scan contours (air-filled tunnel buried in sand with backgrounds removed) [10]

These simulations show how measured GPR data can be faithfully modeled in FDTD and how FDTD simulations can be used to model a GPR system's performance. It shows that the FDTD model produces Typical B-scan contours and the extracted hyperbolas for the tunnel example that can be seen in Figure 5 with the background reflection at the air/sand interface removed. Four angles are selected for 3D B-scan simulation:  $0^\circ$ ,  $\approx 23.96^\circ$ ,  $45^\circ$  and  $\approx 53.13^\circ$ . The hyperbolas extracted from the B-scan simulations were compared to a library of hyperbolas generated by 2D FDTD to determine the angle of the GPR waves travel path. By comparing the angles from the simulations with measured data, these angles were found to produce the B-scans that most closely match the measured ones. The results are summarized in Table 2. The determined angles are well matched to the actual angles. Again, and as expected, the case of  $\theta = 45^\circ$  results in the largest error in determined  $\theta$ .<sup>10</sup>

Table 2. Tunnel Example Correlation Results

3D simulation angle, $\theta$	Best 2D correlation	Maximum error (Distance from tunnel in $s$ -direction)	Mean error
$0^\circ$	$0^\circ$	180.0 ps at 2.25 m	73.9 ps
$\arctan(4/9) \approx 23.96^\circ$	$24^\circ$	93.8 ps at 2.63 m	38.0 ps
$45^\circ$	$24^\circ$	152.1 ps at 3.39 m	47.8 ps
$\text{Arctan}(4/3) \approx 53.13^\circ$	$54^\circ$	535.9 ps at 4.0 mm	206.2 ps

## 5 Simulation Results

**Dependence on Frequency:** System analysis begins by selecting one input and determining its effect of the system's performance. If one extends the analysis of system inputs to the effects of frequency on the depth and resolution like that presented by GST<sup>11</sup>, the results shown in Table 3 show the relationship between resolution, "blind" zone and reflection depth with reference to the antenna used. The simulated measurements are made in a media whose relative dielectric permittivity,  $\epsilon_r = 4.0$  and the specific attenuation is 1 to 2 dB/m. Reflection depth is the detection depth of a flat boundary with reflectance equal to 1.

Table 3. Frequency Dependence [10]

Parameter	Antenna						
	2	900	500	300	150	75	37
Frequency (MHz)	2	900	500	300	150	75	37
Resolution (m)	0.06-0.1	0.2	0.5	1.0	1.0	2.0	4.0
"Blind" zone (m)	0.08	0.1-0.2	0.25-0.5	0.5-1.0	1.0	2.0	4.0
Depth (m)	1.5-2	3-5	7-10	10-15	7-10	10-15	15-30

**Controlling Conductivity:** The 1D-FDTD model allows one to investigate the effect of controlling one variable at a time. Figure 6 shows the results of a FDTD simulation where the specific conductance,  $\sigma$ , of the media is controlled and set to 5.0 Siemens/meter, the relative electrical permittivity,  $\epsilon_r$ , set to 1.0, the frequency set to 2 GHz, and with a grid dimension of  $dx = 0.75$  cm or 20 divisions per wavelength. The figure shows the attenuation of the fields in time.

**Controlling Permittivity:** Another example of system analysis by controlling one variable at a time is the constituent property of permittivity. Permittivity is a property that describes the ability of the media to store electric charge. It can also affect the frequency, wavelength, or amount of energy that is transmitted or reflected.

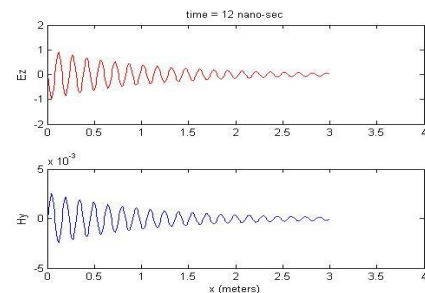


Figure 6. Example of Controlling Sigma.

The table presented within Figure 7 presents the relative permittivity of a number of common earth media. A graphic showing the boundaries and reflections from layers of different permittivity is also included. The reflection and transmission of the electromagnetic waves at each earth

media layer interface depends upon the difference of the permittivity of each layer. The signal received by the GPR receive antenna sub-system is a mixture of the reflection and delays propagating through the multi-layer paths. A representative profile for the different layers is presented.

Material	Relative Permittivity
Air	1
Water	80
Ice	3.14
Dry Snow	1.5-3
Wet Snow	Depends on moisture, particle size
Dry Soil	2 - 4
Dry Sand	3 - 5

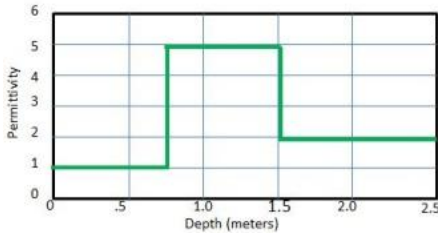
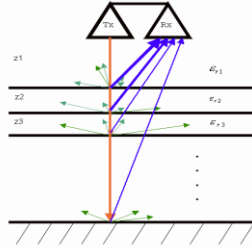


Figure 7. Controlling Permittivity

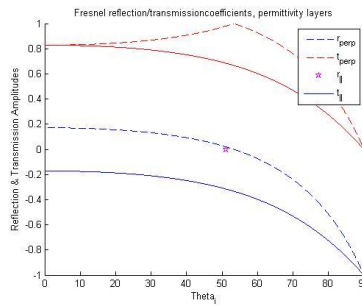


Figure 8. Fresnel reflection and transmission coefficients

The reflection and transmission coefficients for two layers with relative permittivity's of  $\epsilon_{r1} = 2.0$  and  $\epsilon_{r2} = 4.0$  is shown in Figure 8. The reflection and transmission amplitude coefficients are shown for both perpendicular and parallel polarizations of EM waves incident from normal to 90 degrees. For  $\epsilon_{r1} = \epsilon_{r2}$ , there is total transmission and no reflection.

Figure 9 shows the ability of the 1D-FDTD simulation to model the effects of different values of permittivity on the propagation of electromagnetic waves. The specific conductance of the media is set to  $\sigma = 0$  Siemens/m and the value of permittivity is controlled at  $\epsilon_r = 1.0$  and  $\epsilon_r = 10$ . The media is nonmagnetic with permeability equal to free space,  $\mu_0$ . The simulation shows how  $\epsilon_r$  affects both the frequency and the speed of propagation. Both graphs show 12 nano-seconds of propagation. The higher the  $\epsilon_r$ , the slower the wave propagates. This delay gives insight into how deep a reflecting target might be if the  $\epsilon_r$  is known or a method to determine the  $\epsilon_r$  if the depth of the reflecting object is known.

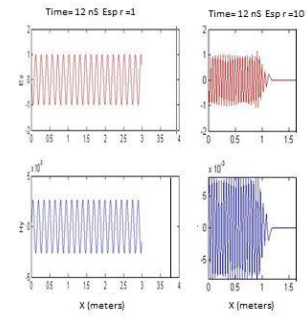


Figure 9. Effect of permittivity on propagation.

This exercise allows one to understand GPR physical processes better by controlling variables that are modeled in the FDTD model. It demonstrates the ability of the model to perform a bistatic polarimetric simulation of the GPR. Using a simple FDTD model and simulation with perfectly matching boundary conditions, a FDTD simulation of rods at half a meter depth was performed. The homogeneous media show the expected result that polarized electromagnetic waves induce larger currents in the direction in which the wave and rod are oriented. Exposed to a polarized EM wave in the x direction, the x-directed rod has larger induced currents in the x-direction, while the y-directed rod has a strong tendency to induce currents in the y-direction if the EM wave is polarized in the y direction. This explains why GPR migration algorithms, developed on a matched-filter response basis, are used to both detect and determine the shape of a buried pipe like object.

Gurel et al presents an excellent example of prism modeling [12]. In Figure 10, the FDTD model simulates two conducting prisms of  $21 \times 21 \times 16$  cells that are buried five cells under the ground, and separated by twenty cells. The A-scan waveforms are calculated and presented next to B-scan results. In Figure 10, the scattering results for a cavity and a dielectric object, with a permittivity of  $\epsilon_r = 1.0$  and  $\epsilon_r = 8$ , respectively, are presented. The two targets are buried twenty cells apart and five cells under the ground that is modeled with a relative permittivity of  $\epsilon_r = 4.0$ . Figure 10 illustrates the typical A-scan and B-scans expected and the ability of the FDTD model to simulate the GPR performance. In Figure 11(a) the targets are dielectric object and a cavity in the ground. Note that the amount of reflection from the two objects closely follows the Fresnel reflection and transmission coefficients illustrated in Figure 7 for layers with the values of  $\epsilon_r = 4.0$  for the soil and  $\epsilon_r = 8$  for the dielectric object and  $\epsilon_r = 4.0$  for the soil and  $\epsilon_r = 1$  for the void. This results in the return from the cavity being larger than the return from the dielectric object. The results of this FDTD simulation are consistent with those using Fresnel reflection and transmission coefficients to calculate the reflection from the objects.

In the second simulation, the dielectric object is replaced by a conducting prism. The reflection from the perfectly conducting prism is nearly 100% and much larger than that of the cavity.

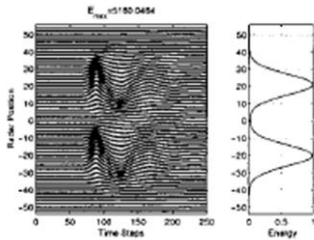


Figure 10. Two perfectly conducting prisms buried 5 cells under the ground and separated by 20 cells [12]

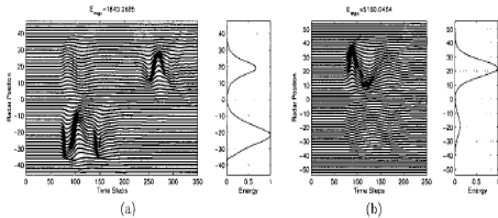


Figure 11. Two objects buried 5 cells under the ground and separated by 20 cells. (a) a cavity and a dielectric object and (b) a cavity and a perfectly conducting prism [12].

These TDFD models and simulations clearly show how the researcher can vary the media and targets buried in the media and systematically evaluate the GPR's performance. These experimental results yield the conclusion that the FDTD technique can be used to accurately simulate the GPR measurements and to faithfully analyze GPR data.

## 6 Conclusions and Future Plans

The initial results presented in this paper demonstrate the ability of the 3D FDTD method to model and simulate the effects of several media on the propagation of GPR signals. It is an important step in the system engineering analysis to identify GPR system deficiencies and what can be done to improve the system's performance. GPR computer models and FDTD simulations provide insight into how GPR systems including their signal processing algorithms perform to detect and identify objects buried under the ground. The TDFD model and simulations described in the paper allow the researcher to vary the media and targets buried in the media and systematically evaluate the GPR's performance. The effectiveness of the algorithms for data acquisition, signal processing and image processing for target detection and identification can be evaluated. Results from this modeling demonstrate the possibility of future use of this methodology for algorithm development and refinement that will better characterize and expand the trade space with valid GPR alternatives. The approach of simulating various input variables for an existing GPR using relatively simple 3D FDTD calculations has been demonstrated. The experimental results obtained lead to the conclusion that the FDTD techniques can be successfully used for analysis and parameter optimization of the basic signal processing algorithms in GPR.

Future planned research includes: accounting for the humidity and the inhomogeneity of soils on a GPR's performance to allow the development of robust high-

performance detection algorithms. This includes the modeling of objects other than simple pipes and prisms such as multiple targets, dielectric targets in both homogeneous and anisotropic media. In the research to define appropriate solutions, FDTD has the computational ability to faithfully model a large variety of problem spaces. The propagation and detection of buried objects will be further investigated to obtain a better understanding of how the physical GPR components and processes affect the ability to detect and identify buried objects. Finally, the simulations will be expanded to the antenna-to-air and air-to-ground interfaces in order to better understand the interference paths of direct and ground bounced signals on the signals received from the reflections below the ground.

## References.

- [1] Montgomery, D. C. *Design and Analysis of Experiments, 7<sup>th</sup> edition*. Hoboken, NJ: John Wiley and Sons, 2009.
- [2] Baker, G. S., Jordon, T. E., Pardy, J.. "An Introduction to ground penetrating radar (GPR)." *The Geological Society of America*, (Special Paper 432, 2007): 2
- [3] Fritzsche, M. "Detection of buried landmines using ground penetrating radar." *Proceedings of the SPIE*. 2496 (1995): 100-109.
- [4] Trang, A.H.. "Simulation of mine detection over dry soil, snow, ice, and water." *Proceedings of the SPIE*, 2765 (1996): 430-440.
- [5] Williford, C.F. *Comparison of Absorption and Radiation Boundary Conditions Using a Time-Domain Three-Dimensional Finite Difference Electromagnetic Computer Code*. (1985): Air Force Institute of Technology, Wright-Patterson AFB, OH.
- [6] Yee, K.S.. "Numerical Solution of Initial Boundary Value Problems Involving Maxwell's Equation in Isotropic Media," *IEEE Transactions on Antennas and Propagation*. AP-14 (May 1966): 302-307.
- [7] Rymes, M.D. *T3DFD User's Manual: Final Technical Report, August 1979--June 1981*.
- [8] Hebert, J.L. Sanchez-Castro, C. *Implementation of a Three-Dimensional Finite Difference Electromagnetic Code for Analysis of Lightning Interaction with a FAA CV-580 Aircraft*, Wright-Patterson AFB, OH. May 1987.
- [9] Williford C., Jost, R.J., Hebert, J.L. "Comparison of Absorption and Radiation Boundary Conditions in 3DFD Code." *Proceedings of 1986 International Aerospace and Ground Conference on Lightning and Static Electricity*. (1986): 44-1--44-10.
- [10] Belli, K., Rappaport, C., Udall, C., Hines, M., Wadia-Fascetti, S. "Use of 2D FDTD Simulation and the Determination of the GPR Travel Path Angle for Oblique B Scans of 2D Geometries." *Geoscience and Remote Sensing Symposium 2010 IEEE International*. (2010).
- [11] "An Introduction to GPR" Global Scan Technologies. April 2012. <http://www.gstdubai.com/Download/GPR.pdf>.
- [12] Gürel, L. "Simulations of Ground-Penetrating Radars Over Lossy and Heterogeneous Grounds" *IEEE Transactions on Geoscience and Remote Sensing*. 39.6. (2011): 1190-1197.
- [13] Hakim, A. "The dual Yee-cell FDTD scheme." April 2012. <http://ammar-hakim.org/sj/je/je7/je7-dual-yee.html#>.